

Gravitational Wave Imprint of New Symmetry Breaking

Wei Chao^{a,*}, Wen-Feng Cui^{b,†}, Huai-Ke Guo^{b,‡}, Jing Shu^{b,c,d,§}

^aCenter for Advanced Quantum Studies, Department of Physics, Beijing Normal University,
Beijing, 100875, China

^bCAS Key Laboratory of Theoretical Physics, Institute of Theoretical Physics,
Chinese Academy of Sciences, Beijing 100190, China

^c CAS Center for Excellence in Particle Physics, Beijing 100049, China

^d School of Physical Sciences, University of Chinese Academy of Sciences, Beijing 100190, P. R. China

Abstract

It is believed that there are extra fundamental gauge symmetries beyond these described by the Standard Model of particle physics. The scale of these new gauge symmetries are usually too high to be reachable by particle colliders. Considering that the phase transition (PT) relating to the spontaneous breaking of new gauge symmetries to the electroweak symmetry might be strongly first order, we propose in this paper taking the stochastic gravitational waves (GW) arising from this phase transition as an indirect way of detecting these new fundamental gauge symmetries. As an illustration, we explore the possibility of detecting the stochastic GW generated from the PT of $\mathbf{B} - \mathbf{L}$ in the space-based interferometer detectors. Our study shows that the GW energy spectrum is reachable by the LISA, BBO, Taiji and DECIGO experiments only for the case where the spontaneous breaking of $\mathbf{B} - \mathbf{L}$ is triggered by at least two electroweak singlet scalars.

1 Introduction

Although predictions of the Standard Model (SM) of particle physics remarkably agree with almost all experimental observations, we never stop exploring new fundamental gauge symmetries beyond these described by the SM, which are usually motivated by the neutrino masses, dark matter, baryon asymmetry of the universe and the gauge couplings unification

*Email address: chaowei@bnu.edu.cn

†Email address: cuiwenfeng@itp.ac.cn

‡Email address: ghk@itp.ac.cn

§Email address: jshu@itp.ac.cn

at a Grand Unified Theory (GUT). Scales relevant to the spontaneous breaking of new symmetries are usually too high to be accessible by colliders in a foreseeable future. How to probe them is an open question.

The observation of Gravitational Wave (GW) signal at the Laser Interferometer Gravitational Wave Observer (LIGO) [1] has opened a new window to explore the universe and various mysteries of particle physics [2–14]. There are usually two sources of GW [4]: (1) cosmological origin, such as inflation and phase transition (PT); (2) relativistic astrophysical origin (Binary systems etc.). If phase transitions related to the spontaneous breaking of the new gauge symmetries are strongly first order, bubbles of broken phase may nucleate in the background of symmetric phase when the universe cools down to the bubble nucleation temperature. Bubbles expand, collide, merge and finally fill the whole universe to finish the PT, and stochastic GW signals can be generated via the bubble collisions, sound waves after the bubble collision and turbulent motion of bulk fluid [15]. In this paper we propose taking GW as an indirect way of exploring new gauge symmetries, supposing the PT of new gauge symmetry breaking is strongly first order.

Considering the complexity of the non-Abelian gauge group extended models, we study GWs generated from PTs of Abelian gauge group extended models in this paper. There are many possible $U(1)$ extensions of the SM [16], of which gauged $\mathbf{B} - \mathbf{L}$ [17–19], \mathbf{B} , \mathbf{L} [20–22], $\mathbf{B} + \mathbf{L}$ [23, 24], $\mathbf{L}_i - \mathbf{L}_j$ [25] (Here \mathbf{B} and \mathbf{L} are the baryon number and lepton number, respectively) have received great attentions. Since $U(1)_{\mathbf{B}-\mathbf{L}}$ only need minimal extensions to the SM for anomalies cancellation, it is believed to be the most natural one according to Occam’s Razor¹. We investigate conditions for the bubble nucleation during the PT of $U(1)_{\mathbf{B}-\mathbf{L}}$, then calculate the energy spectrum of GWs generated from this process. Notice that the higher the energy scale of PT is, the larger peak frequency of GW energy spectrum it has [27]. If $U(1)$ is broken at the TeV scale, its GW can be detected at the space-based laser interferometer detectors such as the Laser Interferometer Space Antenna(LISA), Big Bang Observer (BBO), Taiji and Tianqin projects. Alternatively if $U(1)$ is broken at a scale approaching to the GUT, its GW is sensitive to the ground-based Laser interferometer such as aLIGO. Our results show that it is difficult to get large enough GW energy spectrum reachable by the space-based Laser interferometer if the $\mathbf{B} - \mathbf{L}$ is broken by only one electroweak scalar singlet. Alternatively if $\mathbf{B} - \mathbf{L}$ is broken by at least two electroweak scalar singlets, its GW energy spectrum is detectable by the LISA detector, ALIA, DECIGO, BBO and Ultimate-DECIGO. For GWs from the spontaneous breaking of non-Abelian symmetries, we refer the reader to Ref. [28] for the case of 3-3-1 model [29, 30].

The remaining of the paper is organized as follows: In section 2 we give a brief introduction to the Abelian gauge group extensions to the SM and describe the $U(1)_{\mathbf{B}-\mathbf{L}}$ model in detail. Section 3 is focused on the GW signals from the PT of $U(1)_{\mathbf{B}-\mathbf{L}}$. The last part is concluding remarks.

¹Notice that the $U(1)_{\mathbf{R}}$ [26], the gauge symmetry for right-handed fermions, shares the same merit as $U(1)_{\mathbf{B}-\mathbf{L}}$ on anomalies cancellation, but this model is severely constrained by the $Z - Z'$ mixing.

scenario	Abelian symmetries	Q_L	ℓ_L	U_R	D_R	E_R	N_R	H	Φ	Δ
(a)	$\mathbf{B} - \mathbf{L}$	1/3	-1	1/3	1/3	-1	-1	0	2	
(b)	$\mathbf{B} - \mathbf{L}$	1/3	-1	1/3	1/3	-1	-1	0	2	1

Table 1: Quantum numbers of fields under the $U(1)_{\mathbf{B}-\mathbf{L}}$, where Φ and Δ is an electroweak scalar singlet.

2 Abelian gauge group extensions to the SM

Many $U(1)$ extensions to the SM have been proposed in recent years, often with the motivation of resolving problems in cosmology and astrophysics. There are two ways to construct a gauged $U(1)$ symmetry: top-down approach and bottom up approach. A typical example of top-down approach is $U(1)$ from the E_6 GUT [31]. At the GUT scale, E_6 can be broken directly into $SU(3)_C \times SU(2)_L \times U(1)_Y \times U(1)_\psi \times U(1)_\chi$ via the Hosotani mechanism [32]. Some phenomena inspired $U(1)$, such as $\mathbf{L}_i - \mathbf{L}_j$, general $U(1)$ [33], $U(1)_N$ [34–36], etc., are constructed from the bottom-up approach, while $\mathbf{B} - \mathbf{L}$ can be constructed from both approaches. Notice that new fermions are needed for anomalies cancellation of new Abelian gauge symmetry. Of various $U(1)$ models, $\mathbf{B} - \mathbf{L}$ only requires minimal extensions of the SM with three right-handed neutrinos, so we study its property of PT and derivative GW spectrum for simplicity. There are usually two types of $\mathbf{B} - \mathbf{L}$ relating to the pattern of symmetry breaking: one electroweak singlet triggered and two electroweak singlets scalar triggered $\mathbf{B} - \mathbf{L}$ breaking. We list in table. 1 patterns of $\mathbf{B} - \mathbf{L}$, particle contents as well as their charges under $\mathbf{B} - \mathbf{L}$, where N_R represents right-handed neutrino, Φ and Δ are electroweak singlet scalars, respectively. In this paper we assume Φ , Δ and Z' are much heavier than the electroweak scale, such that the PT relating to new Abelian symmetry and electroweak symmetries breaking can be treated separately.

2.1 Model (a)

The Higgs potential for the scenario (a) of $U(1)_{\mathbf{B}-\mathbf{L}}$ can be written as

$$V_0^{(a)} = -\mu_\Phi^2 \Phi^\dagger \Phi + \kappa (\Phi^\dagger \Phi)^2, \quad (1)$$

where $\Phi = (\phi + iG_\Phi + v_\Phi)/\sqrt{2}$, with v_Φ the vacuum expectation value (VEV) of Φ . The two parameters μ_Φ^2 and κ can be replaced by the physical parameters v_ϕ and m_ϕ , $\mu_\Phi^2 = m_\phi^2/2$, $\kappa = m_\phi^2/2v_\phi^2$. In addition, Yukawa interactions of N_R are

$$\mathcal{L}_Y \sim y_N \overline{N_R^C} \Phi N_R + y_N \overline{\ell_L} \tilde{H} N_R + \text{h.c.}, \quad (2)$$

where y_N is 3×3 symmetric Yukawa coupling matrix. The first term generates Majorana masses for right-handed neutrinos as Φ gets non-zero VEV. The tiny but non-zero active neutrino masses arise from the type-I seesaw mechanism [37].

scenario (a)		sceinario (b)	
fields	masses	fields	masses
ϕ	$-\mu_\Phi^2 + 3\kappa\phi^2$	ϕ	$-\mu_\Phi^2 + 3\kappa\phi^2 + \frac{1}{2}\kappa_2\delta^2$
χ	$-\mu_\Phi^2 + \kappa\phi^2$	χ	$-\mu_\Phi^2 + \kappa\phi^2 + \frac{1}{2}\kappa_2\delta^2$
N	$y_N^2\phi^2$	N	$y_N^2\phi^2$
Z'	$4g_{\mathbf{B-L}}^2\phi^2$	Z'	$g_{\mathbf{B-L}}^2(4\phi^2 + \delta^2)$
		δ	$-\mu_\Delta^2 + 3\kappa_1\delta^2 + \frac{1}{2}\kappa_2\phi^2$
		χ'	$-\mu_\Delta^2 + \kappa_1\delta^2 + \frac{1}{2}\kappa_2\phi^2$

Table 2: *Field-dependent masses of various particles..*

To study properties of the PT, one needs the effective potential at the finite temperature in terms of background field ϕ ,

$$\begin{aligned}
V_{\text{eff}} &= V_0 + V_{\text{CW}} + V_T + V_{\text{Daisy}} \\
&= -\frac{1}{2}\mu_\Phi^2\phi^2 + \frac{1}{4}\kappa\phi^4 + \frac{1}{64\pi^2} \sum_i (-1)^{2s_i} n_i m_i^4(\phi) \left(\log \frac{m_i^2(\phi)}{\mu^2} - C_i \right) \\
&+ \frac{T^4}{2\pi^2} \left\{ \sum_{i \in B} n_i J_B \left[\frac{m_i^2(\phi)}{T^2} \right] - \sum_{j \in F} n_j J_F \left[\frac{m_j^2(\phi)}{T^2} \right] \right\} \\
&+ \frac{T}{12\pi} \sum_i n_i \left\{ [m_i^2(\phi)]^{3/2} - [m_i^2(\phi) + \Pi_i(T)]^{3/2} \right\}, \tag{3}
\end{aligned}$$

where V_0 is $V_0^{(a)}$ in terms of background field, V_{CW} known as the Coleman-Weinberg potential at the zero temperature, contains one-loop contributions to the effective potential at the zero temperature, V_T and V_{Daisy} include the one-loop and the bosonic ring contributions at the finite temperature, n_i and s_i are the number of degrees of freedom and the spin of the i -th particle, C_i equals to 5/6 for gauge bosons and 3/2 for scalars and fermions. Eq. (3) is derived in the Landau gauge. It should be noted that the effective potential is gauge dependent and a gauge invariant treatment of the effective potential is still unknown. We refer the reader to Ref. [38] for a gauge independent approach to the electroweak PT. Thermal masses of scalar singlet ϕ and gauge boson Z' are given by

$$\Pi_\phi^{(a)} = \left(\frac{g_{\mathbf{B-L}}^2}{2} + \frac{\kappa}{3} + \frac{y_N^2}{8} \right) T^2, \tag{4}$$

$$\Pi_{Z'}^{(a)} = \frac{5}{3} g_{\mathbf{B-L}}^2 T^2, \tag{5}$$

where $g_{\mathbf{B-L}}$ is the gauge coupling of $U(1)_{\mathbf{B-L}}$. We list in the Table. 2 the field dependent masses of various particles. One can see from Eq. (3) that the cubic term in the effective potential mainly come from the loop contribution of Z' , such that there is strong correlation between the collider constraints on the $g_{\mathbf{B-L}}$, $m_{Z'}$ and the strength of the PT.

2.2 Model (b)

The correlation of Z' with the PT can be loosed in the scenario (b), where an extra scalar singlet, $\Delta \equiv (\delta + v_\Delta + i\chi')/\sqrt{2}$, is included. For this scenario, the tree-level potential can be written as

$$V_0^{(b)} = -\mu_\Phi^2 \Phi^\dagger \Phi + \kappa(\Phi^\dagger \Phi)^2 - \mu_\Delta^2 \Delta^\dagger \Delta + \kappa_1(\Delta^\dagger \Delta)^2 + \kappa_2(\Phi^\dagger \Phi)(\Delta^\dagger \Delta) + \{\Lambda \Delta^2 \Phi^\dagger + \text{h.c.}\}, \quad (6)$$

where Λ is a coupling with energy scale. μ_Φ^2 and μ_Δ^2 can be replaced with v_ϕ and v_δ via the tadpole conditions

$$\mu_\phi^2 = \frac{1}{2}\kappa_2 v_\delta^2 + \kappa v_\phi^2 + \frac{\Lambda v_\delta^2}{\sqrt{2}v_\phi}, \quad (7)$$

$$\mu_\Delta^2 = \kappa_1 v_\delta^2 + \frac{1}{2}\kappa_2 v_\phi^2 + \sqrt{2}\Lambda v_\phi. \quad (8)$$

The mass matrix for the CP-even scalars follows,

$$\mathcal{M}_{\phi,\delta}^2 = \begin{pmatrix} 2v_\phi^2 \kappa - \frac{v_\delta^2 \Lambda}{\sqrt{2}v_\phi} & v_\delta(v_\phi \kappa_2 + \sqrt{2}\Lambda) \\ v_\delta(v_\phi \kappa_2 + \sqrt{2}\Lambda) & 2v_\delta^2 \kappa_1 \end{pmatrix}, \quad (9)$$

which can be diagonalized by a 2×2 orthogonal matrix parametrized by a rotation angle θ ,

$$s_1 = c_\theta \phi + s_\theta \delta, \quad s_2 = -s_\theta \phi + c_\theta \delta, \quad (10)$$

where $s_{1,2}$ are mass eigenstates with mass eigenvalues m_{s_1} and m_{s_2} respectively. Three quartic couplings can now be written in term of physical parameters,

$$\kappa_1 = \frac{m_{s_1}^2 s_\theta^2 + m_{s_2}^2 c_\theta^2}{2v_\theta^2}, \quad (11)$$

$$\kappa_2 = \frac{s_\theta c_\theta (m_{s_1}^2 - m_{s_2}^2) - \sqrt{2}\Lambda v_\delta}{v_\delta v_\phi}, \quad (12)$$

$$\kappa = \frac{2m_{s_1}^2 c_\theta^2 v_\phi + 2m_{s_2}^2 s_\theta^2 v_\phi + \sqrt{2}\Lambda v_\delta^2}{4v_\phi^3}. \quad (13)$$

For the CP-odd scalars, their mass matrix is given by

$$\mathcal{M}_{G_\phi, \chi'}^2 = -\frac{\Lambda}{\sqrt{2}v_\phi} \begin{pmatrix} v_\delta^2 & -2v_\delta v_\phi \\ -2v_\delta v_\phi & 4v_\phi^2 \end{pmatrix}. \quad (14)$$

It can be diagonalized by a rotation matrix with angle $\theta' = \arctan[v_\delta/(2v_\phi)]$ and gives the following mass eigenstates

$$G_{Z'} = c_{\theta'} G_\phi + s_{\theta'} \chi', \quad A = -s_{\theta'} G_\phi + c_{\theta'} \chi', \quad (15)$$

where $G_{Z'}$ is the Goldstone boson and A is the physical CP-odd scalar with its mass given by $m_A^2 = -\Lambda(v_\delta^2 + 4v_\phi^2)/\sqrt{2}v_\phi$, which implies $\Lambda < 0$. The physical parameters in this scenario are then

$$v_\phi, \quad v_\delta, \quad m_{s_1}, \quad m_{s_2}, \quad \theta, \quad \Lambda. \quad (16)$$

The effective potential of the scenario (b) has the same form as Eq. (3) up to the following replacements: $(a) \rightarrow (b)$, $m_i(\phi) \rightarrow m_i(\phi, \delta)$. The field dependent masses are tabulated in the second column of Table. 2, while the thermal masses of the various fields are given below,

$$\Pi_\phi^{(b)} = \left(\frac{g_{\mathbf{B-L}}^2}{2} + \frac{\kappa}{3} + \frac{\kappa_2}{12} + \frac{y_N^2}{8} \right) T^2, \quad (17)$$

$$\Pi_\delta^{(b)} = \left(\frac{g_{\mathbf{B-L}}^2}{4} + \frac{\kappa_1}{3} + \frac{\kappa_1}{12} \right) T^2, \quad (18)$$

$$\Pi_{Z'}^{(b)} = \frac{7}{4} g_{\mathbf{B-L}}^2 T^2. \quad (19)$$

With these inputs, the phase history can be analyzed. A particular advantage of model(b) is that there is a cubic term in Eq. (6) at the tree-level, which can generate a barrier between the broken and symmetric phases without the aid of loop corrections. As a result it is easier to get a first order PT for this scenario, compared with model(a) where the barrier is provided by Z' from loop corrections.

We now address collider constraints on the Z' mass. A heavy Z' with SM Z couplings to fermions was searched at the LHC in the dilepton channel, which is excluded at the 95% CL for $M_{Z'} < 2.9$ TeV from the ATLAS [39] and for $M_{Z'} < 2.79$ TeV from the CMS [40]. The measurement of $e^+e^- \rightarrow f\bar{f}$ above the Z-pole at the LEP-II puts lower bound on $M_{Z'}/g_{\text{new}}$, which is about 6 TeV [41]. Further constraint is given by the ATLAS collaboration [42] with 36.1 fb^{-1} of proton-proton collision data collected at $\sqrt{s} = 13$ TeV, which has $M_{Z_{\mathbf{B-L}}} > 4.2$ TeV. We keep these constraints in studying PTs of these models.

3 Gravitational wave signals

For parameter settings of these two models that can give a first order phase transition, there will be gravitational waves generated, mainly coming from three processes: bubble collisions, sound waves in the plasma and Magnetohydrodynamic turbulence(see Ref. [4, 15, 43] for recent reviews). The total energy spectrum can be written approximately as the sum of these three contributions:

$$\Omega_{\text{GW}} h^2 \simeq \Omega_{\text{col}} h^2 + \Omega_{\text{sw}} h^2 + \Omega_{\text{turb}} h^2, \quad (20)$$

where the Hubble constant is defined following the conventional way $H = 100h \text{ kms}^{-1}\text{Mpc}^{-1}$. The energy spectrums depend on three important input parameters for each specific par-

ticle physics model: the bubble wall velocity($\equiv v_w$),

$$\alpha = \frac{\Delta\rho}{\pi^2 g_* T^4/30} \Big|_{T=T_n}, \quad \text{and} \quad \beta = H_n T_n \frac{d(S_3/T)}{dT} \Big|_{T=T_n}, \quad (21)$$

where $\Delta\rho$ is the difference of energy density between the false and true vacua, g_* is the number of relativistic degrees of freedom and H_n is the Hubble constant evaluated at the nucleation temperature T_n , which corresponds approximately to the temperature when $S_3(T)/T = 140$ [44]. The parameter α characterizes the strength of the PT while β denotes roughly the inverse time duration of the PT. With these parameters solved numerically, one can obtain the energy spectrum of the gravitational waves for three sources.

Firstly for the GW from the bubble collision, it can be calculated using the envelop approximation [45–47] either by numerical simulations [48] or by a recent analytical approximation [49]. Both results can be summarized in the following form,

$$\Omega_{col} h^2 = 1.67 \times 10^{-5} \Delta(v_w) \left(\frac{H_n}{\beta} \right)^2 \left(\frac{\kappa_\phi \alpha}{1 + \alpha} \right)^2 \left(\frac{100}{g_*} \right)^{1/3} S_{\text{env}}(f). \quad (22)$$

Here κ_ϕ is the fraction of latent heat transferred to the scalar field gradient, $\Delta(v_w)$ is a numerical factor and S_{env} captures the spectral shape dependence. The two different treatments by Ref. [49] and Ref. [48] lead to slightly different results on the $\Delta(v_w)$ and S_{env} . We adopt here the results from the numerical simulation,

$$\Delta(v_w) = \frac{0.48 v_w^3}{1 + 5.3 v_w^2 + 5 v_w^4}, \quad S_{\text{env}} = \frac{3.8 (f/f_{\text{env}})^{2.8}}{1 + 2.8 (f/f_{\text{env}})^{3.8}}, \quad (23)$$

with f_{env} the peak frequency at present time given by,

$$f_{\text{env}} = 16.5 \times 10^{-6} \left(\frac{f_*}{\beta} \right) \left(\frac{\beta}{H_n} \right) \left(\frac{T_n}{100 \text{ GeV}} \right) \left(\frac{g_*}{100} \right)^{1/6} \text{ Hz}, \quad (24)$$

which is the redshifted frequency of the peak frequency, f_* , at the time of the PT,

$$f_* = \frac{0.62}{1.8 - 0.1 v_w + v_w^2}. \quad (25)$$

For the spectral shape S_{env} , the analytical treatment in Ref. [49] shows the correct behavior for low frequency $S_{\text{env}} \propto f^3$ required by causality [50] while the result from the numerical simulations differs from this one in a minor way. According to a more recent paper [51], in which the runaway conclusion [52] of the bubble expansion is ruled-out, the energy deposited in the scalar field is negligible and should be neglected in GW calculations. We therefore neglect the contribution of bubble collision due to the smallness of κ_ϕ .

Secondly, the bulk motion of the fluid in the form of sound wave are produced after the bubble collisions. It also generates GWs and the energy spectrum has been simulated, with [53],

$$\Omega_{\text{sw}} h^2 = 2.65 \times 10^{-6} \left(\frac{H_n}{\beta} \right)^2 \left(\frac{\kappa_v \alpha}{1 + \alpha} \right)^2 \left(\frac{100}{g_*} \right)^{1/3} v_w \left(\frac{f}{f_{\text{sw}}} \right)^3 \left(\frac{7}{4 + 3(f/f_{\text{sw}})^2} \right)^{7/2}. \quad (26)$$

Here f_{sw} is the peak frequency at current time redshifted from the one at the phase transition: $2\beta/(\sqrt{3}v_w)$, then

$$f_{\text{sw}} = 1.9 \times 10^{-5} \frac{1}{v_w} \left(\frac{\beta}{H_n} \right) \left(\frac{T_n}{100 \text{ GeV}} \right) \left(\frac{g_*}{100} \right)^{1/6} \text{ Hz}. \quad (27)$$

Similar to κ_ϕ , the factor κ_v is the fraction of latent heat transformed into the bulk motion of the fluid. We use the method summarized in Ref. [54] to calculate κ_v as a function of (α, v_w) and note that a fitted approximate formula is given in Ref. [54]. We also note that a more recent numerical simulation by the same collaboration [55] gives a slightly enhanced $\Omega_{\text{sw}} h^2$ and a slightly reduced peak frequency f_{sw} .

Finally the plasma at the time of phase transition is fully ionized and the resulting MHD turbulence can give another source of GWs. Neglecting a possible helical component [56], the generated GW spectrum can be modeled in a similar way [57, 58],

$$\Omega_{\text{turb}} h^2 = 3.35 \times 10^{-4} \left(\frac{H_n}{\beta} \right)^2 \left(\frac{\kappa_{\text{turb}} \alpha}{1 + \alpha} \right)^{3/2} \left(\frac{100}{g_*} \right)^{1/3} v_w \frac{(f/f_{\text{turb}})^3}{[1 + (f/f_{\text{turb}})]^{11/3} (1 + 8\pi f/h_*)}, \quad (28)$$

with the peak frequency f_{turb} given by,

$$f_{\text{turb}} = 2.7 \times 10^{-5} \frac{1}{v_w} \left(\frac{\beta}{H_n} \right) \left(\frac{T_n}{100 \text{ GeV}} \right) \left(\frac{g_*}{100} \right)^{1/6} \text{ Hz}. \quad (29)$$

We need to know the factor κ_{turb} which is the fraction of latent heat transferred to MHD turbulence. The precise value is still undetermined and a recent numerical simulation shows that κ_{turb} can be parametrized as $\kappa_{\text{turb}} \approx \epsilon \kappa_v$, where the numerical factor ϵ varying roughly between $5 \sim 10\%$ [53]. Here we take tentatively $\epsilon = 0.1$.

For detection of the GWs, one needs to compare these spectrums with the sensitivity curve of each detector. The LISA detector [59] is currently the most mature experiment and the recently finished LISA pathfinder has confirmed its design goals. We therefore consider the sensitivities of the four LISA configurations N2A5M5L6(C1), N2A1M5L6(C2), N2A2M5L4(C3), N1A1M2L4(C4) presented in Ref. [15, 60], which include the instrumental noise of the LISA detector obtained using the detector simulation package LISACode [61] as well as the astrophysical foreground from the compact white dwarf binaries in our Galaxy. We also consider the discovery prospect of several other proposed experiments:

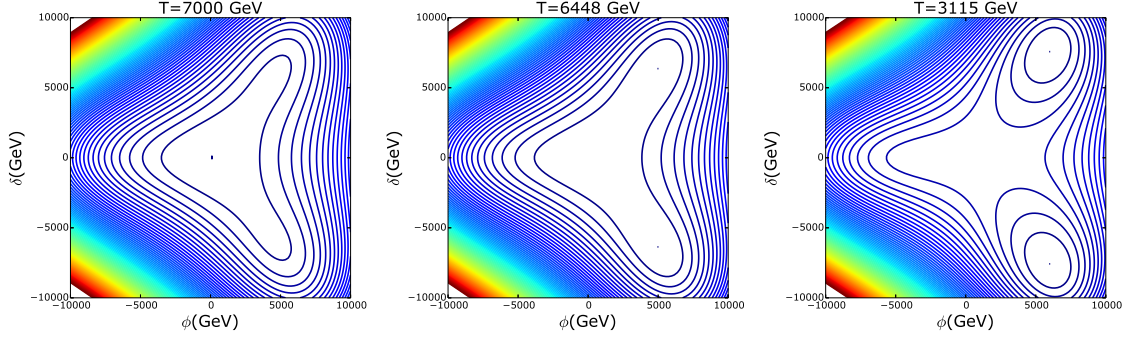


Figure 1: The contours of the effective potential of model(b) at three typical temperatures, with blue lines for lower values and red for higher values. The left figure is at a temperature higher than $T_C \approx 6448\text{GeV}$, the middle one is at T_C and the right figure is at $T_n \approx 3115\text{GeV}$. The benchmark parameters are chosen as: $v_\phi = 4637\text{GeV}$, $v_\delta = 1902\text{GeV}$, $\theta = 0.128$, $m_{s_1} = 2400\text{GeV}$, $m_{s_2} = 1236\text{GeV}$ and $\Lambda = -2143\text{GeV}$.

the Advanced Laser Interferometer Antenna (ALIA) [62]², the Big Bang Observer(BBO), the DECI-hertz Interferometer Gravitational wave Observatory(DECIGO) ³ and Ultimate-DECIGO [63].

We implement two **B – L** models in CosmoTransitions [64] which traces the phase history of each model, locates the critical temperature T_C and gives the bounce solutions to obtain the bubble nucleation temperature T_n . We then use these outputs to calculate the GW energy spectrums and compare them with the listed detector sensitivities.

From an extensive scan over the parameter space of model(a) at the mass scale of $\mathcal{O}(\text{TeV})$, we find that a first order PT can occur for a significant proportion of their parameter spaces. However, the resulting GW signals are generally too weak to be discovered where the most optimistic case can marginally be reached by the Ultimate-DECIGO. This is due to the relatively large values of β and small values of α obtained, aside from the enhanced $\mathcal{O}(\text{TeV})$ temperature, which reduce the magnitude of GW energy spectrum as well as pushing the peak frequency to higher values. On the other hand, for the parameter space at the electroweak scale, the GWs can generally be reached by most detectors, which is however ruled by collider searches of Z' .

Model(b) has a sizable parameter space where the generated GWs from PT falls within the sensitive regions of various detectors, due to the easily realized PT from the tree level barrier with the aid of a negative cubic term in the effective potential in Eq. 6. We show a benchmark point from this parameter space and present the details of the PT and the GW spectrum. This benchmark parameter point is $v_\phi = 4637\text{GeV}$, $v_\delta = 1902\text{GeV}$, $\theta = 0.128$, $m_{s_1} = 2400\text{GeV}$, $m_{s_2} = 1236\text{GeV}$ and $\Lambda = -2143\text{GeV}$. For this case, the minima in the field space (ϕ, δ) lie in the direction $\phi > 0$, where the cubic term in Eq. 6 is negative.

²It is now renamed as Taiji.

³The ALIA, BBO and DECIGO sensitivity data are taken from the website <http://rhcole.com/apps/GWplotter/>

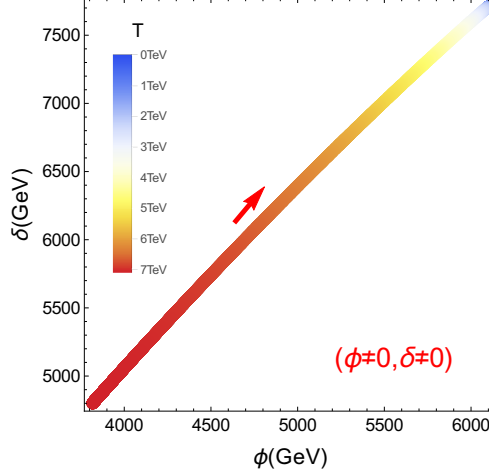


Figure 2: The tracks of the minimum ($\phi \neq 0, \delta \neq 0$) in the (ϕ, δ) plane with the colors showing the value of temperature, which can be read from the colormap on the left.

Due to the reflection symmetry $\delta \rightarrow -\delta$, this occur in a pair. The shape of the effective potential is shown as contours in Fig. 1 where hot regions have larger values of V while cold regions have smaller values. The leftest figure shows the shape at a relatively high temperature where the universe sits at its origin and the two minima in direction $\phi > 0$ are developing. As T drops to the critical temperature $T_C \approx 6448\text{GeV}$, these two minima become degenerate with the one at the origin as shown in the middle figure. As T further drops below the critical temperature, the broken phase begin to nucleate on the background of symmetric phase at $T_n \approx 3115\text{GeV}$, which corresponds to the rightest figure. The details on the evolution of the new phase is shown in Fig. 2 in the plane (ϕ, δ) where the arrow denotes the direction of time flow and the colors show the value of temperature.

To calculate the GWs from this model, we need the input κ_v which we calculate following Ref. [54]. For benchmark given in Fig. 1, we find $\alpha = 0.09$ and κ_v depends on one free parameter v_w . For different values of v_w , the motion of the plasma surrounding the bubble takes different forms and the value of κ_v is shown in the left panel of Fig. 3, where representative points are selected marked as A, B, C and D shown as green points in the figure. The velocity profiles of the plasma is shown in the right panel of Fig. 3 as a function of r/t , where r is the radial distance from the bubble center and t starts at T_n . For case A, v_w is smaller than the sound speed in the plasma ($\equiv c_s = 1/\sqrt{3}$, the vertical dashed line in left panel), and the bubble proceeds as deflagrations, with a velocity profile shown by the dotted lines in the right panel. For case B, v_w is larger than c_s , a rarefaction wave develops behind the bubble wall, yet the fluid has non-zero velocity ahead of the wall, corresponding to the solid lines in the right panel. This falls within the hybrid region of the left panel, denoting supersonic deflagration [65]. For case C, v_w is increased to the Jouguet detonation [66] (the magenta dotted line in the left panel) and the velocity of the fluid ahead of the wall becomes zero, corresponding to the dashed line in the right panel. For

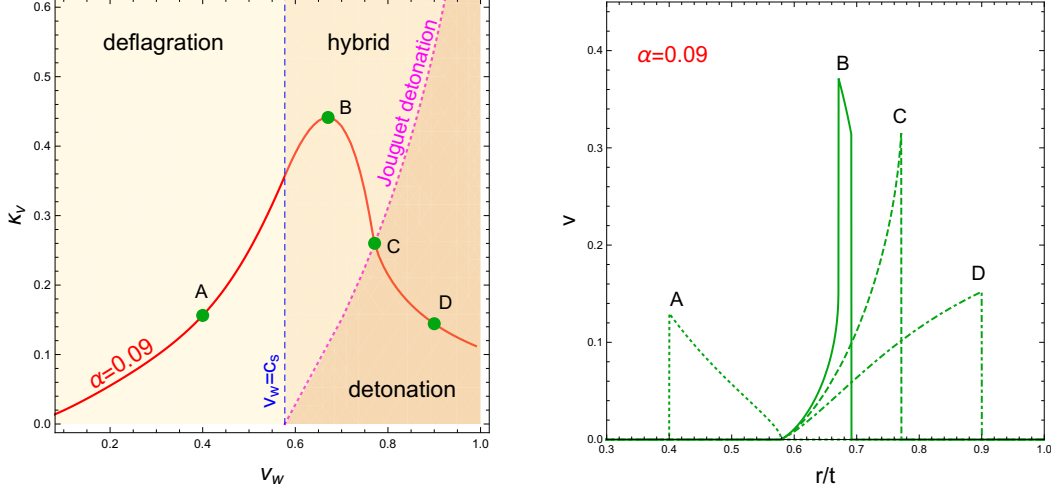


Figure 3: Left panel: The red line shows the fraction of latent heat transferred to the bulk motion of the plasma κ_v when the bubble wall velocity is varied for $\alpha = 0.09$, which is derived the benchmark in Fig. 1. Also plotted here are the deflagration, hybrid (supersonic deflagration) and detonation regions characterizing the dynamics of the phase transition, separated by the blue dashed line (when v_w is equal to the sound speed of the relativistic plasma $c_s = 1/\sqrt{3}$) and the magenta dotted line (Jouguet detonation). Four representative cases: A, B, C and D, marked with green points, are chosen to calculate the GW spectra. Right panel: the velocity profile as a function of r/t for the four representative cases of the left panel plot.

case D, the bubble wall velocity gets larger and the expansion takes the form of detonation with the profile shown by the dot-dashed line in the right panel.

The resulting GW energy spectrums for these four points from sound waves (blue dashed) and turbulence (brown dotted) are shown in Fig. 4, where their sum corresponds to the red solid line. The color-shaded regions at the top are the experimental sensitivity regions for the four LISA configurations C1-C4 (red), ALIA (gray), DECIGO (yellow), BBO (green) and Ultimate-DECIGO (purple). It is observed that for all four cases, the spectrum at around the peak frequency is dominated by sound waves while turbulence becomes more important for large and small frequencies. The total GW spectra all fall within the experimental sensitive regions of the LISA configurations C1, C2, C3 as well as other experiments. For case B, corresponding to the peak of κ_v in the left panel of Fig. 3, the least sensitive configuration of LISA C4 can also reach some proportion of the GW spectrum even though the resulting signal-to-noise ratio might be too small.

To assess the discovery prospect of the GWs, we quantify the detectability of the GWs using the signal-to-noise ratio adopted in Ref. [15]:

$$\text{SNR} = \sqrt{\mathcal{T} \int_{f_{\min}}^{f_{\max}} df \left[\frac{h^2 \Omega_{\text{GW}}(f)}{h^2 \Omega_{\text{exp}}(f)} \right]^2}, \quad (30)$$

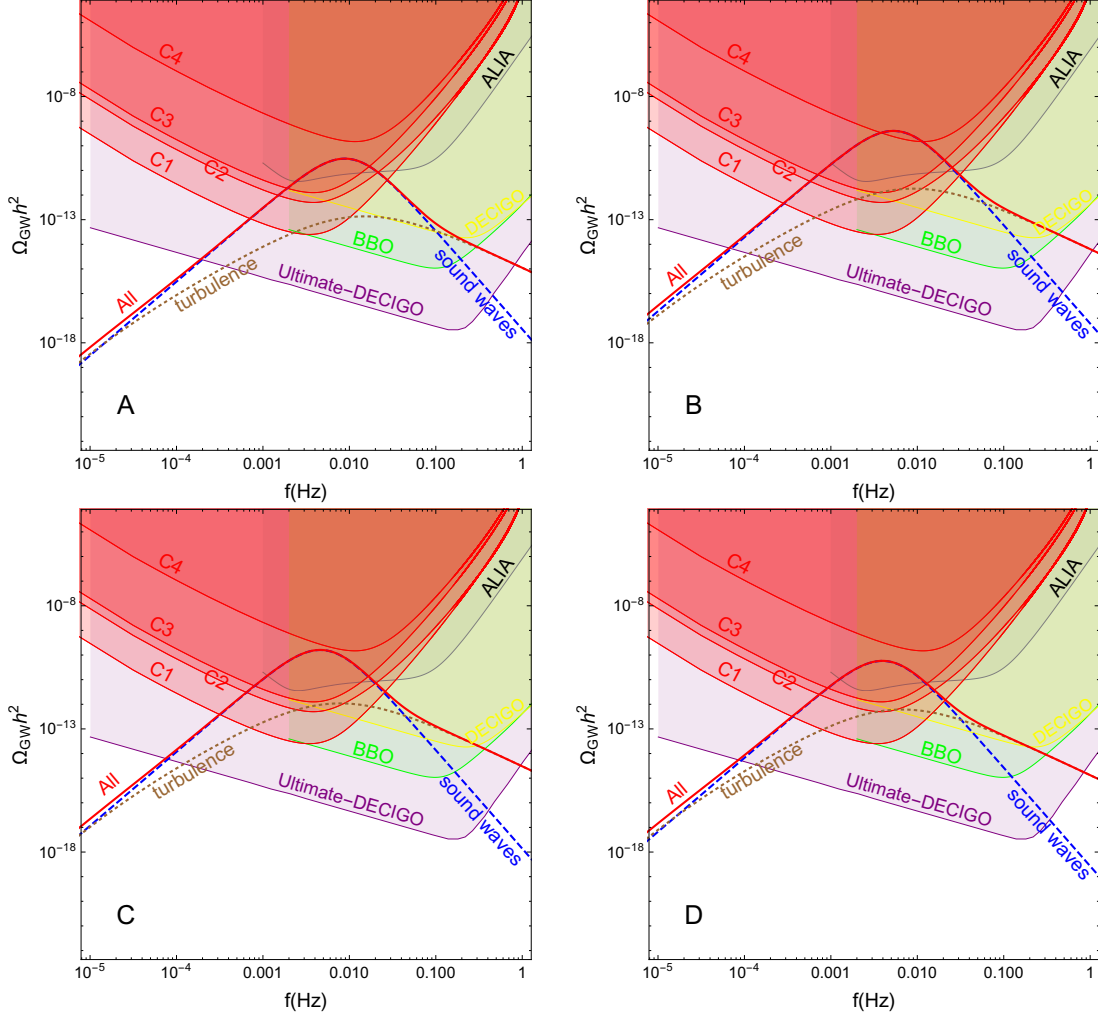


Figure 4: The GW energy spectrum as the function of its frequency for the benchmark in Fig. 1 and four representative bubble wall velocities (the four green points A, B, C and D in Fig. 3). The individual contributions from sound waves and turbulence are plotted using blue dashed, brown dotted lines respectively, with their sum corresponding to the red solid line. Also plotted are the experimental sensitive regions at the top, corresponding to color-shaded regions, from four configurations of the LISA detector C1-C4 (red), ALIA (gray), DECIGO (yellow), BBO (green) and Ultimate-DECIGO (purple).

where $h^2 \Omega_{\text{exp}}$ is the experimental sensitivity shown in Fig. 4 and \mathcal{T} is the mission duration of the experiment in years. With this formula, we calculate SNR as a function of v_w for each experiment and show the results in Fig. 5. We also show two representative SNR thresholds $\text{SNR}_{\text{thr}} = 10, 50$ as suggested by Ref. [15] with horizontal black lines for comparison. From this figure, we can see that all SNR curves have a peak at $v_w \approx 0.67$. This peak corresponds to the maximum of $\kappa_v \approx 0.44$ in the left panel of Fig. 3, represented by case B in previous discussions, which has supersonic deflagration profile of the plasma surrounding the bubble.

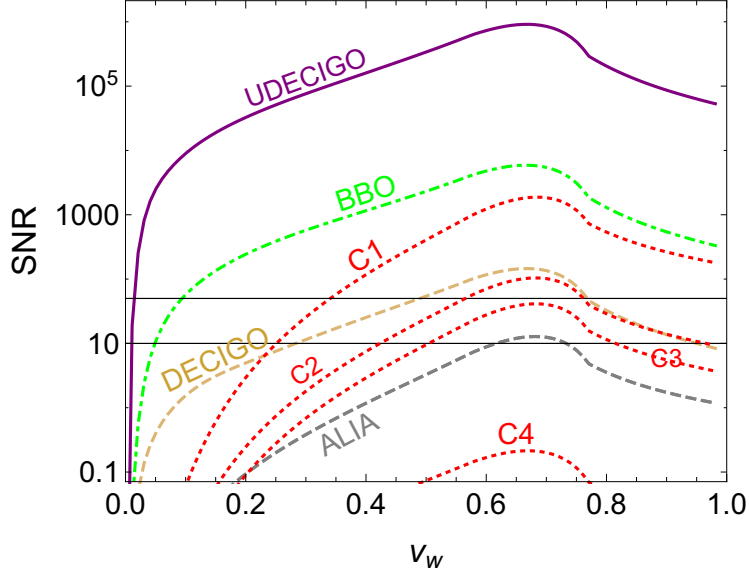


Figure 5: The SNR as the function of bubble wall velocity v_w for the benchmark point in model(b) using the different experimental sensitivity inputs. Two black horizontal lines denote the SNR threshold values 10 and 50 respectively.

It is clear from this figure that for a wide range of v_w , the SNR for the LISA configuration C1, BBO and UDECIGO is above the two thresholds $\text{SNR}_{\text{thr}} = 10, 50$. For DECIGO, there is also a range $0.5 \lesssim v_w < 0.8$ above the threshold 50 and this range becomes much wider for the threshold 10. For the LISA configuration C2 with six links, the GW for a wide range $0.4 < v_w < 1.0$ is above the threshold value 10 and can therefore be detected according to Ref. [15]. For the LISA configurations C3 and C4, both of which have four links, the uncorrelated noise reduction technique used in the six-link cases is not available and therefore the SNR needs to be larger than 50 to be detectable [15]. So in this case, the GW is not reachable by C3 and C4 for any v_w . For ALIA, there is a window at $v_w \approx 0.7$ where the SNR is above 10.

4 Discussion

The discovery of GW at the LIGO initiates a new era in high energy physics and gravity. In this paper we propose the stochastic GW as an indirect way of probing the spontaneous breaking new gauge symmetry beyond the SM. Working in models with gauged $\mathbf{B} - \mathbf{L}$ extension of the SM, we studied the strength of PT relating to the spontaneous breaking of the $\mathbf{B} - \mathbf{L}$ as well as the stochastic GW signals generated during the same PT in the space based interferometer. We find that the power spectrum of GW generated is reachable by the LISA, BBO, ALIA, DECIGO and Ultimate-DECIGO for the case where the spontaneous breaking of $\mathbf{B} - \mathbf{L}$ is triggered by at least two electroweak scalar singlets. It should be

mentioned that there is no way to identify its intrinsic physics if any stochastic GW signal is observed. But it provides a guidance for new physics hunters since stochastic GW signal with peak frequency at near 0.01 Hz is a hint of new scalar interactions or new symmetry at the TeV scale. This work make sense on this point of view. Although we only focused on the $U(1)$ case in this paper, our studies can be easily extended to the non-Abelian case since it contains all ingredients for the GW calculation.

Acknowledgements

JS is supported by the National Natural Science Foundation of China under grant No.11647601, No.11690022 and No.11675243 and also supported by the Strategic Priority Research Program of the Chinese Academy of Sciences under grant No.XDB23030100.

References

- [1] B. P. Abbott, et al., Binary Black Hole Mergers in the first Advanced LIGO Observing Run, *Phys. Rev. X* 6 (4) (2016) 041015. [arXiv:1606.04856](#), [doi:10.1103/PhysRevX.6.041015](#).
- [2] I. P. Ivanov, Building and testing models with extended Higgs sectors, *Prog. Part. Nucl. Phys.* 95 (2017) 160–208. [arXiv:1702.03776](#), [doi:10.1016/j.ppnp.2017.03.001](#).
- [3] A. Beniwal, M. Lewicki, J. D. Wells, M. White, A. G. Williams, Gravitational wave, collider and dark matter signals from a scalar singlet electroweak baryogenesis [arXiv:1702.06124](#).
- [4] R.-G. Cai, Z. Cao, Z.-K. Guo, S.-J. Wang, T. Yang, The Gravitational-Wave Physics [arXiv:1703.00187](#), [doi:10.1093/nsr/nwx029](#).
- [5] A. Addazi, A. Marciano, Gravitational waves from dark first order phase transitions and dark photons [arXiv:1703.03248](#).
- [6] K. Tsumura, M. Yamada, Y. Yamaguchi, Gravitational wave from dark sector with dark pion [arXiv:1704.00219](#), [doi:10.1088/1475-7516/2017/07/044](#).
- [7] Z. Kang, P. Ko, T. Matsui, Strong First Order EWPT and Strong Gravitational Waves in Z_3 -symmetric Singlet Scalar Extension [arXiv:1706.09721](#).
- [8] W. Chao, CP Violation at the Finite Temperature [arXiv:1706.01041](#).
- [9] L. Bian, H.-K. Guo, J. Shu, Gravitational Waves, baryon asymmetry of the universe and electric dipole moment in the CP-violating NMSSM [arXiv:1704.02488](#).

- [10] F. P. Huang, J.-H. Yu, Explore Inert Dark Matter Blind Spots with Gravitational Wave Signatures [arXiv:1704.04201](#).
- [11] A. Addazi, A. Marciano, Limiting Majoron self-interactions from Gravitational waves experiments [arXiv:1705.08346](#).
- [12] L. Marzola, A. Racioppi, V. Vaskonen, Phase transition and gravitational wave phenomenology of scalar conformal extensions of the Standard Model, *Eur. Phys. J. C* 77 (7) (2017) 484. [arXiv:1704.01034](#), doi:10.1140/epjc/s10052-017-4996-1.
- [13] C.-W. Chiang, E. Senaha, On gauge dependence of gravitational waves from a first-order phase transition in classical scale-invariant $U(1)'$ models [arXiv:1707.06765](#).
- [14] W. Chao, H.-K. Guo, J. Shu, Gravitational Wave Signals of Electroweak Phase Transition Triggered by Dark Matter [arXiv:1702.02698](#).
- [15] C. Caprini, et al., Science with the space-based interferometer eLISA. II: Gravitational waves from cosmological phase transitions, *JCAP* 1604 (04) (2016) 001. [arXiv:1512.06239](#), doi:10.1088/1475-7516/2016/04/001.
- [16] P. Langacker, The Physics of Heavy Z' Gauge Bosons, *Rev. Mod. Phys.* 81 (2009) 1199–1228. [arXiv:0801.1345](#), doi:10.1103/RevModPhys.81.1199.
- [17] R. N. Mohapatra, R. E. Marshak, Local B-L Symmetry of Electroweak Interactions, Majorana Neutrinos and Neutron Oscillations, *Phys. Rev. Lett.* 44 (1980) 1316–1319, [Erratum: *Phys. Rev. Lett.* 44, 1643 (1980)]. doi:10.1103/PhysRevLett.44.1316.
- [18] R. E. Marshak, R. N. Mohapatra, Quark - Lepton Symmetry and B-L as the $U(1)$ Generator of the Electroweak Symmetry Group, *Phys. Lett.* 91B (1980) 222–224. doi:10.1016/0370-2693(80)90436-0.
- [19] C. Wetterich, Neutrino Masses and the Scale of B-L Violation, *Nucl. Phys. B* 187 (1981) 343–375. doi:10.1016/0550-3213(81)90279-0.
- [20] P. Fileviez Perez, M. B. Wise, Baryon and lepton number as local gauge symmetries, *Phys. Rev. D* 82 (2010) 011901, [Erratum: *Phys. Rev. D* 82, 079901 (2010)]. [arXiv:1002.1754](#), doi:10.1103/PhysRevD.82.079901, 10.1103/PhysRevD.82.011901.
- [21] T. R. Dulaney, P. Fileviez Perez, M. B. Wise, Dark Matter, Baryon Asymmetry, and Spontaneous B and L Breaking, *Phys. Rev. D* 83 (2011) 023520. [arXiv:1005.0617](#), doi:10.1103/PhysRevD.83.023520.
- [22] W. Chao, Pure Leptonic Gauge Symmetry, Neutrino Masses and Dark Matter, *Phys. Lett. B* 695 (2011) 157–161. [arXiv:1005.1024](#), doi:10.1016/j.physletb.2010.10.056.

- [23] W. Chao, Symmetries behind the 750 GeV diphoton excess, *Phys. Rev. D* **93** (11) (2016) 115013. [arXiv:1512.06297](#), [doi:10.1103/PhysRevD.93.115013](#).
- [24] W. Chao, H.-k. Guo, Y. Zhang, Majorana Dark matter with B+L gauge symmetry, *JHEP* **04** (2017) 034. [arXiv:1604.01771](#), [doi:10.1007/JHEP04\(2017\)034](#).
- [25] X.-G. He, G. C. Joshi, H. Lew, R. R. Volkas, Simplest Z-prime model, *Phys. Rev. D* **44** (1991) 2118–2132. [doi:10.1103/PhysRevD.44.2118](#).
- [26] W. Chao, Phenomenology of the gauge symmetry for right-handed fermions [arXiv:1707.07858](#).
- [27] P. S. B. Dev, A. Mazumdar, Probing the Scale of New Physics by Advanced LIGO/VIRGO, *Phys. Rev. D* **93** (10) (2016) 104001. [arXiv:1602.04203](#), [doi:10.1103/PhysRevD.93.104001](#).
- [28] F. P. Huang, X. Zhang, Probing the hidden gauge symmetry breaking through the phase transition gravitational waves [arXiv:1701.04338](#).
- [29] F. Pisano, V. Pleitez, An $SU(3) \times U(1)$ model for electroweak interactions, *Phys. Rev. D* **46** (1992) 410–417. [arXiv:hep-ph/9206242](#), [doi:10.1103/PhysRevD.46.410](#).
- [30] P. H. Frampton, Chiral dilepton model and the flavor question, *Phys. Rev. Lett.* **69** (1992) 2889–2891. [doi:10.1103/PhysRevLett.69.2889](#).
- [31] S. F. King, S. Moretti, R. Nevzorov, Theory and phenomenology of an exceptional supersymmetric standard model, *Phys. Rev. D* **73** (2006) 035009. [arXiv:hep-ph/0510419](#), [doi:10.1103/PhysRevD.73.035009](#).
- [32] Y. Hosotani, Dynamical Mass Generation by Compact Extra Dimensions, *Phys. Lett.* **126B** (1983) 309–313. [doi:10.1016/0370-2693\(83\)90170-3](#).
- [33] T. Appelquist, B. A. Dobrescu, A. R. Hopper, Nonexotic neutral gauge bosons, *Phys. Rev. D* **68** (2003) 035012. [arXiv:hep-ph/0212073](#), [doi:10.1103/PhysRevD.68.035012](#).
- [34] W. Chao, Dark matter, LFV and neutrino magnetic moment in the radiative seesaw model with fermion triplet, *Int. J. Mod. Phys. A* **30** (01) (2015) 1550007. [arXiv:1202.6394](#), [doi:10.1142/S0217751X15500074](#).
- [35] W. Chao, M. J. Ramsey-Musolf, Hidden from view: Neutrino masses, dark matter, and TeV-scale leptogenesis in a neutrinophilic two-Higgs-doublet model, *Phys. Rev. D* **89** (3) (2014) 033007. [arXiv:1212.5709](#), [doi:10.1103/PhysRevD.89.033007](#).

- [36] Y. Cai, W. Chao, The Higgs Seesaw Induced Neutrino Masses and Dark Matter, *Phys. Lett. B* 749 (2015) 458–463. [arXiv:1408.6064](#), [doi:10.1016/j.physletb.2015.08.026](#).
- [37] P. Minkowski, $\mu \rightarrow e\gamma$ at a Rate of One Out of 10^9 Muon Decays?, *Phys. Lett.* 67B (1977) 421–428. [doi:10.1016/0370-2693\(77\)90435-X](#).
- [38] H. H. Patel, M. J. Ramsey-Musolf, Baryon Washout, Electroweak Phase Transition, and Perturbation Theory, *JHEP* 07 (2011) 029. [arXiv:1101.4665](#), [doi:10.1007/JHEP07\(2011\)029](#).
- [39] G. Aad, et al., Search for high-mass dilepton resonances in pp collisions at $\sqrt{s} = 8$ TeV with the ATLAS detector, *Phys. Rev. D* 90 (5) (2014) 052005. [arXiv:1405.4123](#), [doi:10.1103/PhysRevD.90.052005](#).
- [40] V. Khachatryan, et al., Search for physics beyond the standard model in dilepton mass spectra in proton-proton collisions at $\sqrt{s} = 8$ TeV, *JHEP* 04 (2015) 025. [arXiv:1412.6302](#), [doi:10.1007/JHEP04\(2015\)025](#).
- [41] M. Carena, A. Daleo, B. A. Dobrescu, T. M. P. Tait, Z' gauge bosons at the Tevatron, *Phys. Rev. D* 70 (2004) 093009. [arXiv:hep-ph/0408098](#), [doi:10.1103/PhysRevD.70.093009](#).
- [42] M. Aaboud, et al., Search for new high-mass phenomena in the dilepton final state using 36.1 fb^{-1} of proton-proton collision data at $\sqrt{s} = 13$ TeV with the ATLAS detector [arXiv:1707.02424](#).
- [43] D. J. Weir, Gravitational waves from a first order electroweak phase transition: a review, 2017. [arXiv:1705.01783](#).
URL <http://inspirehep.net/record/1598112/files/arXiv:1705.01783.pdf>
- [44] R. Apreda, M. Maggiore, A. Nicolis, A. Riotto, Gravitational waves from electroweak phase transitions, *Nucl. Phys. B* 631 (2002) 342–368. [arXiv:gr-qc/0107033](#), [doi:10.1016/S0550-3213\(02\)00264-X](#).
- [45] A. Kosowsky, M. S. Turner, R. Watkins, Gravitational radiation from colliding vacuum bubbles, *Phys. Rev. D* 45 (1992) 4514–4535. [doi:10.1103/PhysRevD.45.4514](#).
- [46] A. Kosowsky, M. S. Turner, R. Watkins, Gravitational waves from first order cosmological phase transitions, *Phys. Rev. Lett.* 69 (1992) 2026–2029. [doi:10.1103/PhysRevLett.69.2026](#).
- [47] A. Kosowsky, M. S. Turner, Gravitational radiation from colliding vacuum bubbles: envelope approximation to many bubble collisions, *Phys. Rev. D* 47 (1993) 4372–4391. [arXiv:astro-ph/9211004](#), [doi:10.1103/PhysRevD.47.4372](#).

- [48] S. J. Huber, T. Konstandin, Gravitational Wave Production by Collisions: More Bubbles, JCAP 0809 (2008) 022. [arXiv:0806.1828](#), [doi:10.1088/1475-7516/2008/09/022](#).
- [49] R. Jinno, M. Takimoto, Gravitational waves from bubble collisions: An analytic derivation, Phys. Rev. D95 (2) (2017) 024009. [arXiv:1605.01403](#), [doi:10.1103/PhysRevD.95.024009](#).
- [50] C. Caprini, R. Durrer, T. Konstandin, G. Servant, General Properties of the Gravitational Wave Spectrum from Phase Transitions, Phys. Rev. D79 (2009) 083519. [arXiv:0901.1661](#), [doi:10.1103/PhysRevD.79.083519](#).
- [51] D. Bodeker, G. D. Moore, Electroweak Bubble Wall Speed Limit, JCAP 1705 (05) (2017) 025. [arXiv:1703.08215](#), [doi:10.1088/1475-7516/2017/05/025](#).
- [52] D. Bodeker, G. D. Moore, Can electroweak bubble walls run away?, JCAP 0905 (2009) 009. [arXiv:0903.4099](#), [doi:10.1088/1475-7516/2009/05/009](#).
- [53] M. Hindmarsh, S. J. Huber, K. Rummukainen, D. J. Weir, Numerical simulations of acoustically generated gravitational waves at a first order phase transition, Phys. Rev. D92 (12) (2015) 123009. [arXiv:1504.03291](#), [doi:10.1103/PhysRevD.92.123009](#).
- [54] J. R. Espinosa, T. Konstandin, J. M. No, G. Servant, Energy Budget of Cosmological First-order Phase Transitions, JCAP 1006 (2010) 028. [arXiv:1004.4187](#), [doi:10.1088/1475-7516/2010/06/028](#).
- [55] M. Hindmarsh, S. J. Huber, K. Rummukainen, D. J. Weir, Shape of the acoustic gravitational wave power spectrum from a first order phase transition [arXiv:1704.05871](#).
- [56] T. Kahniashvili, L. Campanelli, G. Gogoberidze, Y. Maravin, B. Ratra, Gravitational Radiation from Primordial Helical Inverse Cascade MHD Turbulence, Phys. Rev. D78 (2008) 123006, [Erratum: Phys. Rev.D79,109901(2009)]. [arXiv:0809.1899](#), [doi:10.1103/PhysRevD.78.123006](#), [doi:10.1103/PhysRevD.79.109901](#).
- [57] C. Caprini, R. Durrer, G. Servant, The stochastic gravitational wave background from turbulence and magnetic fields generated by a first-order phase transition, JCAP 0912 (2009) 024. [arXiv:0909.0622](#), [doi:10.1088/1475-7516/2009/12/024](#).
- [58] P. Binetruy, A. Bohe, C. Caprini, J.-F. Dufaux, Cosmological Backgrounds of Gravitational Waves and eLISA/NGO: Phase Transitions, Cosmic Strings and Other Sources, JCAP 1206 (2012) 027. [arXiv:1201.0983](#), [doi:10.1088/1475-7516/2012/06/027](#).
- [59] H. Audley, et al., Laser Interferometer Space Antenna [arXiv:1702.00786](#).

- [60] A. Klein, et al., Science with the space-based interferometer eLISA: Supermassive black hole binaries, *Phys. Rev. D* **93** (2) (2016) 024003. [arXiv:1511.05581](#), [doi:10.1103/PhysRevD.93.024003](#).
- [61] A. Petiteau, G. Auger, H. Halloin, O. Jeannin, E. Plagnol, S. Pireaux, T. Regimbau, J.-Y. Vinet, LISACode: A Scientific simulator of LISA, *Phys. Rev. D* **77** (2008) 023002. [arXiv:0802.2023](#), [doi:10.1103/PhysRevD.77.023002](#).
- [62] X. Gong, et al., Descope of the ALIA mission, *J. Phys. Conf. Ser.* **610** (1) (2015) 012011. [arXiv:1410.7296](#), [doi:10.1088/1742-6596/610/1/012011](#).
- [63] H. Kudoh, A. Taruya, T. Hiramatsu, Y. Himemoto, Detecting a gravitational-wave background with next-generation space interferometers, *Phys. Rev. D* **73** (2006) 064006. [arXiv:gr-qc/0511145](#), [doi:10.1103/PhysRevD.73.064006](#).
- [64] C. L. Wainwright, CosmoTransitions: Computing Cosmological Phase Transition Temperatures and Bubble Profiles with Multiple Fields, *Comput. Phys. Commun.* **183** (2012) 2006–2013. [arXiv:1109.4189](#), [doi:10.1016/j.cpc.2012.04.004](#).
- [65] H. Kurki-Suonio, M. Laine, Supersonic deflagrations in cosmological phase transitions, *Phys. Rev. D* **51** (1995) 5431–5437. [arXiv:hep-ph/9501216](#), [doi:10.1103/PhysRevD.51.5431](#).
- [66] P. J. Steinhardt, Relativistic Detonation Waves and Bubble Growth in False Vacuum Decay, *Phys. Rev. D* **25** (1982) 2074. [doi:10.1103/PhysRevD.25.2074](#).